To be published in Optics Express:

Title:	Nonlinear properties of laser-processed polycrystalline silicon waveguides for integrated photonics
Authors:	Ozan Aktas,Stuart MacFarquhar,Swe Oo,Antulio Tarazona,Harold Chong,Anna Peacock
Accepted:	27 August 20
Posted	27 August 20
DOI:	https://doi.org/10.1364/OE.400536

Nonlinear properties of laser-processed polycrystalline silicon waveguides for integrated photonics

Ozan Aktas,[1,*] Stuart J. MacFarquhar,[1] Swe Z. Oo,[2] Antulio Tarazona,[1] Harold M. H. Chong,[2,3] and Anna C. Peacock[1]

[1]*Optoelectronics Research Centre, University of Southampton, Highfield, Southampton, SO17 1BJ, UK.*
[2]*School of Electronics and Computer Science, University of Southampton, Highfield, Southampton, SO17 1BJ, UK.*
[3]*School of Materials Science, Japan Advanced Institute of Science and Technology, Nomi, Ishikawa 923-1292, Japan*
**O.Aktas@soton.ac.uk*

Abstract: We report nonlinear optical characterization of cm-long polycrystalline silicon (poly-Si) waveguides at telecom wavelengths. Laser post-processing of lithographically-patterned amorphous silicon deposited on silica-on-silicon substrates provides low-loss poly-Si waveguides with surface-tension-shaped boundaries. Achieving optical losses as low as 4 dB cm^{-1} enabled us to demonstrate effects of self-phase modulation (SPM) and two-photon absorption (TPA). Analysis of the spectral broadening and nonlinear losses with numerical modeling reveals the best fit values of the Kerr coefficient n_2=4.5×10^{-18} m W^{-1} and TPA coefficient β_{TPA}=9.0×10^{-12} m^2 W^{-1}, which are within the range reported for crystalline silicon. On-chip low-loss poly-Si paves the way for flexible integration of nonlinear components in multi-layered photonic systems.

1. Introduction

Over the last two decades, polycrystalline silicon (poly-Si) has attracted growing interest as a material with great prospects for the convergence of electronics and photonics. Compared to single crystalline silicon (c-Si), poly-Si has the potential to offer similar optical and electrical properties, but can be produced using more flexible deposition methods [1,2]. As a result, back-end integration of active and passive photonic devices with nano-electronics has been demonstrated by using poly-Si as conductive gate electrodes, strip waveguides, modulators and ring resonators [3-5]. However, one area where poly-Si has yet to be exploited is for nonlinear optical applications, primarily due to the relatively high transmission losses (6-7 dB cm^{-1} [6]) compared to its c-Si counterparts (1-2 dB cm^{-1} [7]). This has led to alternative deposited materials, such as low loss hydrogenated amorphous silicon [8] and silicon nitride [9], being explored as nonlinear platforms for integrated systems. However, the drawback of these materials is that they suffer from poor electronic quality. Thus, there is still a great need to develop large grain and low loss poly-Si components that can offer the full complement of functionality required for optoelectronic systems, including nonlinear processing, but which can be produced more flexibly than c-Si devices.

The optical losses in poly-Si are typically characterized by two main contributors. The first is scattering losses due to surface roughness on the etched waveguides associated with the multi-grain structure of the material. The second is scattering due to density fluctuations in the bulk material and absorption by dangling bonds within the grain boundaries. Therefore, various deposition and post-processing methods have been developed to reduce the waveguide losses. Thermal annealing has been applied to increase grain size in poly-Si and

thus reduce the number of grains boundaries [10,11]. On the other hand, hydrogenation has been used to passivate dangling bonds in the grain boundaries [12,13]. Of these approaches, thermal annealing is probably the most popular and has produced waveguides with losses as low as 4.1 dB cm^{-1} with optimization of etching parameters, albeit in structures with relatively large dimensions (several microns in width and height) [14]. However, such annealing methods require long exposure of the whole sample to high temperatures to achieve good crystalline quality, compromising back-end complementary metal-oxide semiconductor (CMOS) compatibility.

Alternatively, laser-based annealing of amorphous silicon (a-Si) has been explored, initially using pulsed UV excimer lasers to treat entire a-Si films before device construction [4], and more recently using a continuous wave (CW) visible laser to process individual waveguides after patterning [15]. This latter approach has the advantage in that the laser heat treatment is highly localized to the individual components, which helps to increase the grain growth within the waveguide regions, resulting in a significant reduction in the transmission losses from 20 dB cm^{-1}, when processing the entire film [4], down to 5.3 dB cm^{-1} [15]. Additionally, the density of defects and the number of dangling bonds in grain boundaries have been found to be smaller in CW laser annealing than those in pulsed excimer laser annealing [16].

In this study, we extend our production of laser-processed poly-Si components and demonstrate their use for nonlinear optical propagation. Scanning electron microscopy (SEM), Raman microscopy, atomic force microscopy (AFM), and cut-back loss measurements were used to assess the quality of the waveguides. Laser melting of the a-Si wires, followed by reflowing and crystallization, results in poly-Si waveguides with smooth surfaces, root mean square (RMS) roughness of 0.5 nm, and propagation losses as low as 4 dB cm^{-1}. These low losses have allowed for the observation of SPM-induced spectral broadening and TPA-induced nonlinear saturation of short pulse propagation. To the best of our knowledge, this is the first nonlinear optical characterization of planar poly-Si waveguides processed by lasers, with the estimated material parameters being in close agreement with values reported for c-Si. Thus, these high optical quality poly-Si waveguides open a route to the flexible integration of nonlinear components in photonic and electronic systems.

2. Fabrication and post-process laser reflowing of silicon waveguides

The sample fabrication begins by thermally growing a 4 μm thick oxide layer on top of a silicon wafer, which acts as a buffer to eliminate optical leakage from the waveguides to the Si substrate. Hot-wire chemical vapor deposition (HWCVD) was then used to deposit a 400 nm thick a-Si film on the top of the silica layer, using a silane (SiH_4) precursor [17]. HWCVD was preferred over other common deposition techniques as it allows for the production of a-Si materials with low hydrogen content at low temperatures, which were set at 320 °C for our sample to be compatible with the CMOS processes. Minimizing the hydrogen concentration is important to eliminate out-diffusion during laser processing. Following the deposition, e-beam lithography and plasma etching were used to pattern the a-Si thin film into straight waveguides with rectangular cross-sections having widths of 3 μm and 4 μm. Pre-patterning the a-Si films enables the confinement of the thermal energy during the subsequent process of laser melting and crystallization [15]. Not only does this reduce the overall thermal budget of the fabrication process, but it also helps to increase the grain growth. This is because the localized heating causes complete melting of the a-Si wires, which promotes directional solidification and liquid phase crystallization from the trailing edge of the travelling molten zone [18].

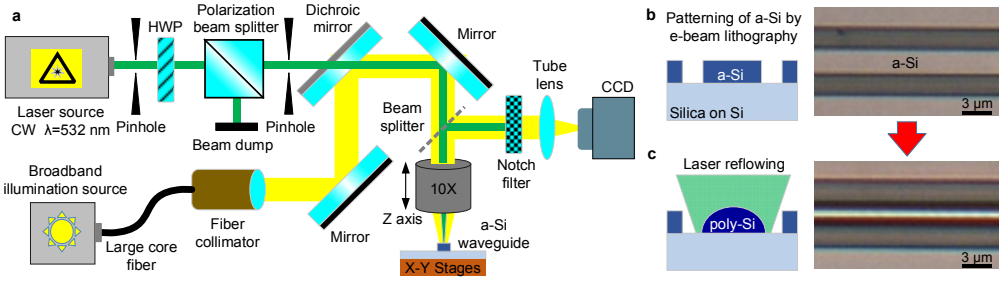

Fig. 1. Laser processing of a-Si waveguides on silica/Si substrates. (**a**) Schematic of the laser processing setup. (**b**) Schematic figure and optical microscope image showing the cross-sectional and top view, respectively, of a patterned a-Si waveguide. (**c**) Schematic figure and optical microscope image showing the reflowed poly-Si waveguide after laser-induced melting.

A schematic of the experimental setup used for laser processing of the pre-patterned a-Si waveguides is shown in Fig. 1(a). An ultra-stable single-frequency laser source (IPG-GLR-10W) emitting CW radiation at a wavelength of 532 nm was used as the thermal source. The laser output was set to a fixed optical power of 1W, and a half-wave plate (HWP) and a polarization beam splitter were used to adjust the optical power in the range of 300-800 mW, as measured after the focusing objective. The laser beam was focused to a spot of size 5 μm in diameter on the surface by a 10× objective lens (NA-0.25), which was enough to cover the whole surface of the patterned waveguides. By adjusting the position of the second lens in front of the CCD camera, we were able to bring the focus of the laser and illumination source to the same point. In situ monitoring allows for initial alignment and focusing of the laser beam on the a-Si waveguides, as well as for detection of partial melting or ablation of the material during processing. The samples were mounted with a vacuum holder on a set of software-controlled 2-axis high precision stages (Aerotech, ABL-1500), which were moved to linearly scan the laser spot along the a-Si waveguides at scan speeds ranging from 0.1 to 10 mm s^{-1} over a 4 cm total displacement. Because of the high optical absorption of a-Si in the visible spectrum, high temperatures, enough to melt the semiconductor material, can be easily reached. Optical microscope images given in Fig. 1(b,c), show the top surface of the waveguides before and after laser reflowing, respectively.

For optimization of the parameters, some test waveguides were first processed with a range of scan speeds and input laser powers. The optimum parameters that yield the best surface quality and crystallinity were then determined using optical microscopy and Raman microscopy, respectively. For laser processing of a-Si waveguides with a width of 3 μm (4 μm), the best combination of scan speed and optical power were found to be 1 mm s^{-1}, and 600 mW (500 mW). For a given fixed beam size, the optimum optical power for processing was found to be close to the ablation threshold of the material, which depends on the width of the waveguide. It is higher for smaller widths due to the smaller absorption cross-section and greater cooling rate. Additionally, laser processing didn't show any dependency on the polarization of the laser beam, which is normally incident on the flat surface of the patterned a-Si waveguides, due to the degeneracy of the polarization, and full melting of the material.

3. Material and surface characterizations of the laser-reflowed waveguides

As can be seen in the SEM micrograph of a laser-processed poly-Si waveguide in Fig. 2(a), localized melting induces a material reflow due to the surface tension of the molten silicon, turning the initially rectangular cross-section into a parabolic cross-section with a height greater than the initial thickness (400 nm) of the a-Si film. Reshaping greatly improves the surface quality, decreasing the initial RMS roughness of 3.5 nm to 0.5 nm, as assessed through AFM surface characterization of a laser-processed 3 μm wide poly-Si waveguide given in Fig. 2(b). Various cross-sectional profiles can be achieved either by adjusting the

ratio of the initial width and height, or by reflowing the waveguide after a partial under-etching. However, near circular cross-sections help to reduce the difference between mode sizes of TM and TE polarized light, and the sensitivity of the transmission on the polarization direction. On the other hand, as the width of the waveguides increases, more parabolic cross sections and higher aspect ratios are reached, increasing the difference between mode sizes, and the transmission through wider waveguides becomes increasingly polarization-dependent. Additionally, the initial rectangular shape can be preserved if the molten semiconductor is encapsulated by a crucible, such as a silica over-cladding deposited on the patterned a-Si waveguides before laser processing. The repeatability of the laser processing depends on the motional capabilities of the stages scanning the samples under the laser beam, and the stability of the optical power emitted by the laser source. Moreover, whilst working in ambient conditions is very practical, all residues and dust must be removed from the surface before commencing the process to avoid damage.

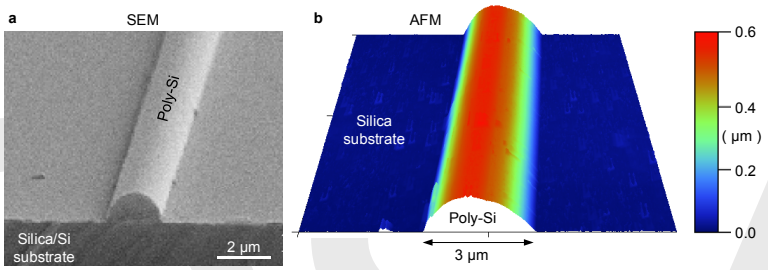

Fig. 2. (**a**) SEM micrograph showing a poly-Si waveguide after laser processing. (**b**) Topographical characterization of a laser-processed 3 µm wide poly-Si waveguide by AFM. The initially rectangular cross-section turns into a parabolic shape. The surface-tension reshaping of the molten Si enables smooth surfaces with a RMS roughness of 0.5 nm.

In order to characterize the crystalline quality of the processed waveguides, micro-focus Raman spectroscopy (Renishaw Invia) was applied before and after laser processing, by using a 50× objective lens (NA-0.75), a Nd:YAG excitation laser source (532 nm, 1 mW) and a silicon grating of 2400 lines/mm. The measurements were taken in the backscattered mode, which is most sensitive to the longitudinal optical (LO) phonon mode of crystalline silicon. Normalized Raman spectra of the as-deposited material (red) and a laser-processed waveguide (blue) are shown in Fig. 3(a). The Raman spectrum of the as-deposited material displays broad peaks which are typical for a-Si. On the other hand, the Raman spectrum of the laser-processed waveguide has a single sharp peak at 517.4 cm^{-1}, which is shifted 2.5 cm^{-1} left from the 519.9 cm^{-1} peak of the c-Si reference, as shown with detail in Fig. 3(b). The c-Si reference peak was first fit by using a Voigt function to determine the Gaussian broadening of the instrument, assuming a Lorentzian line shape with a linewidth of Γ_0=2.7 cm^{-1}, corresponding to the intrinsic response of the c-Si. The Lorentzian line shape of the poly-Si peak was then deconvolved from the experimental data. The linewidth of the poly-Si peak was found to be Γ=2.72±0.11 cm^{-1}, which is almost equal to that of the c-Si reference, indicating very good crystallinity. The laser spot size of the Raman instrument is about 1 µm in diameter, therefore, we expect that the poly-Si waveguides consist of crystal grains with sizes larger than the spot size. Indeed, it has been recently shown using X-ray diffraction that the length of laser-processed crystal grains in a similar structure can be longer than 1 mm [15]. As the poly-Si Raman peak has a symmetrical line shape with a negligible amount of broadening, we attribute the lower wavenumber shift of $\Delta\omega$=-2.5 cm^{-1} to a residual uniaxial tensile strain of ε=0.7 %, which can be calculated via the relation $\Delta\omega = b \times \varepsilon$, where b=-347 cm^{-1} is strain-shift coefficient of the LO Raman mode of silicon [19]. During solidification, the large difference in the thermal expansion coefficients of the molten silicon and silica substrate results in tensile strains, which are comparable to those achieved by laser processing

of Si-Ge alloys on Si using the same setup [20]. Laser-induced residual tensile strains remain uniform along the poly-Si waveguides, due to the thermal steady-state conditions ensured by the constant scan speeds and powers during laser processing, and were observed to be stable at room temperatures for several months, without causing any physical deformation.

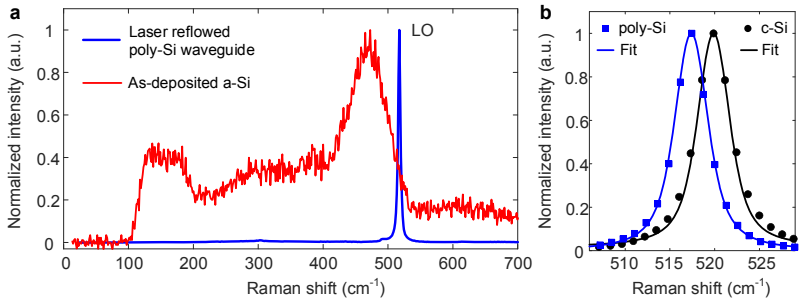

Fig. 3. Material characterization using Raman spectroscopy before and after laser processing. (**a**) Raman spectra showing the transformation from an amorphous state to a polycrystalline state by laser-induced crystallization. (**b**) The shift of the poly-Si peak from the characteristic 519.9 cm^{-1} Raman peak of c-Si, due to the residual tensile stresses after laser processing.

4. Characterization of the linear propagation losses

We start our optical characterization of the laser-processed poly-Si waveguides in the linear regime by using a cut-back technique that requires measuring the insertion losses of waveguides of differing lengths. A schematic of the experimental setup is shown in Fig. 4(a). As a light source, we used a CW diode laser emitting at a wavelength of 1550 nm with a maximum power of 80 mW. The sample used in the experiments consisted of a series of poly-Si waveguides with widths of 3 and 4 µm. To prepare the facets for optical coupling, both ends were cleaved and inspected using a microscope for flatness. The sample was then placed on a 3-axis high precision stage (Thorlabs, MAX301), and TM polarized light was free space coupled in and out of each waveguide by using 60× (NA-0.85) and 40× (NA-0.6) microscope objectives, respectively. Although these micron-sized poly-Si waveguides support multiple modes, careful monitoring of the input and output coupling using infrared (IR) cameras (MicronViewer 7290A) allows for efficient coupling into the fundamental mode. The light from the output facet was collimated and spatially filtered using a pinhole to isolate the mode, eliminating the scattered light. The optical power was measured after the pinhole by using a power meter. Cutback measurements were performed by cleaving the sample at different lengths, but keeping the input facet intact to ensure consistent coupling at each step.

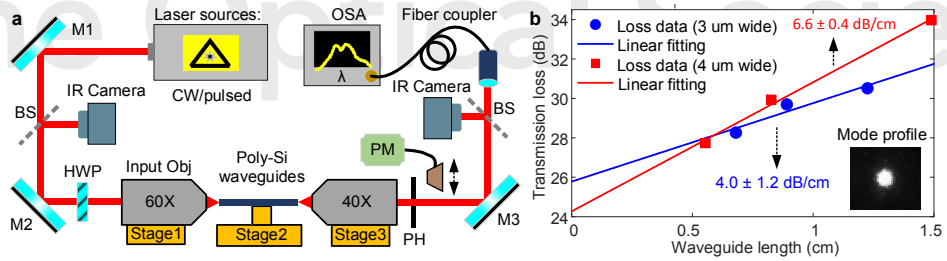

Fig. 4. Characterization of the optical losses in the laser-processed poly-Si waveguides. (**a**) Schematic showing the experimental setup used for the optical characterizations. M, mirror; HWP, half-wave plate; BS, beam splitter; PH, pinhole; OSA, optical spectrum analyzer; PM, power meter. (**b**) Results of the cut-back measurements for transmission losses of the 3 µm (blue) and 4 µm (red) wide waveguides at different lengths, using a 1550 nm wavelength source. Inset figure shows the output mode profile taken by the IR camera.

Results of the cutback measurements are given in Fig. 4(b). The inset image shows the output mode profile captured by an IR camera, revealing the optical mode is well confined by the high refractive index silicon core. The propagation losses, as measured from the slope of the transmission data, were found to be 4.0±1.2 dB cm^{-1} and 6.6±0.4 dB cm^{-1} for the 3 μm (blue) and 4 μm (red) wide poly-Si waveguides, respectively. The waveguides with larger widths were observed to have higher propagation losses, due to the increased number of grain boundaries and reduced crystallinity, particularly at the edges [15,18]. Nevertheless, the propagation losses in the 3 μm waveguides represent an improvement of >1dB cm^{-1} compared to our recent results (5.3 dB cm^{-1}) obtained using a CW Argon-ion laser for the processing [15], which were significantly better than the 20 dB cm^{-1} estimated when using a pulsed excimer laser [4]. We attribute this loss reduction to the improved stability of the laser processing source (< %1 power fluctuations), which allows us to operate very close to the material damage threshold, where grain growth has been shown to be maximal [21]. We routinely achieved low losses for the most of the laser-processed 3 μm wide waveguides (between 4-7 dB cm^{-1}). The y-intercepts of the linear fits to the data correspond to the total optical coupling losses at the front and end facets, which are 25.8±1.1 dB and 24.3±0.5 dB for the 3 μm and 4 μm wide poly-Si waveguides, respectively. In principle, much lower input coupling losses are possible for free space coupling if the angular and positional misalignment of the input beam relative to the facet, and the roughness of the cleaved surfaces, are minimized.

5. Characterization of nonlinear optical properties

5.1 Description of pulse propagation in a poly-Si waveguide

Nonlinear pulse propagation in poly-Si waveguides can be described by a generalized form of the nonlinear Schrödinger equation (NLSE) [22]:

$$\frac{\partial A(z,t)}{\partial z} = -\frac{i\beta_2}{2}\frac{\partial^2 A(z,t)}{\partial t^2} + i\gamma|A(z,t)|^2 A(z,t) - \frac{1}{2}(\alpha_l + \sigma_f)A(z,t). \quad (1)$$

Here, $A(z,t)$ is the pulse envelope, β_2 is the group velocity dispersion (GVD), and γ is the nonlinearity parameter defined as $\gamma = k_0 n_2/A_{eff} + i\beta_{TPA}/2A_{eff}$ in terms of the nonlinear refractive index n_2, TPA coefficient β_{TPA}, and effective mode area A_{eff}. The remaining terms are the linear propagation loss α_l, and the free carrier loss $\alpha_f = \sigma_{FCA}(1 + i\mu)N_c(z,t)$ where α_{FCA} is the coefficient of free carrier absorption (FCA), and μ governs the free-carrier dispersion (FCD), which is estimated as $\mu = 2k_c k_o/\sigma_{FCA}$ with k_c = 1.35×10^{-27} m^{-3} [23]. $N_c(z,t)$ is the density of free carriers generated by TPA, which is described by the rate equation

$$\frac{\partial N_c(z,t)}{\partial t} = \frac{\beta_{TPA}}{2h\nu_0}\frac{|A(z,t)|^4}{A_{eff}^2} - \frac{N_c(z,t)}{\tau_c}, \quad (2)$$

where τ_c is the carrier lifetime, h is the Planck constant, and ν_0 is frequency of the light.

If the dispersion length $L_D = T_0^2/\beta_2$, which is defined in terms of the pulse duration T_0 (assuming a hyperbolic secant $\mathrm{sech}(t/T_0)$ pulse) and GVD parameter β_2, is considerably longer than the waveguide length (L_D>>L_{WG}), it is possible to neglect the effects of dispersion on the pulse propagation. In this case, Eq. (1) can be modified to describe the temporal evolution of the intensity profile, which can be expressed as

$$\frac{\partial I(z,t)}{\partial z} = -\alpha_l I(z,t) - \beta_{TPA} I(z,t)^2 - \sigma_{FCA} N_c(z,t) I(z,t), \quad (3)$$

where $I(z,t) = |A(z,t)|^2/A_{eff}$, which is coupled to Eq. (2). For a given linear loss α_l, Eq. (3) can be used to determine the TPA coefficient β_{TPA} by analyzing the effects of nonlinear loss on the transmission of input pulses with high peak powers.

5.1 Nonlinear transmission losses due to two-photon absorption

To demonstrate the potential of the laser-processed poly-Si waveguides for nonlinear optical applications, we selected the 3 μm wide waveguides, because they have the lowest propagation loss of 4 dB cm^{-1} and a smaller effective mode area A_{eff}. The nonlinear transmission measurements make use of the same experimental setup given in Fig. 4(a), but with the pump source switched to a femtosecond fiber laser (Onefive), which provides hyperbolic secant pulses with a 750 fs full width half maximum (FWHM) duration, operating at 1540 nm, and a repetition rate of 40 MHz. Nonlinear absorption measurements were carried out to investigate the effects of TPA on the high power pulse propagation, as evident by the saturation of the output power seen in Fig. 5(b). The coupled input peak powers were calculated from the measured input average powers for a free space coupling loss of 14 dB per facet, which was estimated from the linear loss measurements above.

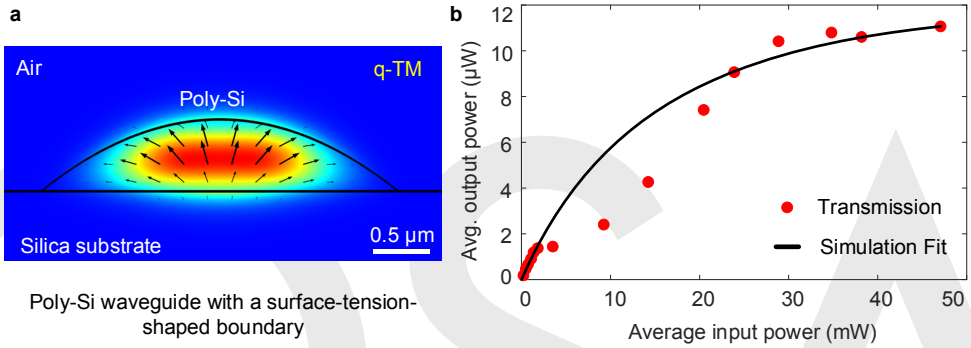

Fig. 5. Characterization of the nonlinear losses. (**a**) Calculated electric field amplitude of the fundamental TM mode for a poly-Si waveguide with a width of 3 μm and height of 0.6 μm. (**b**) Nonlinear saturation of the transmission through the poly-Si waveguide due to TPA.

Mode analysis of the 3 μm wide waveguides was used to calculate the effective area A_{eff}=0.8 μm^2 and the GVD parameter β_2=0.67 $ps^2\,m^{-1}$ at the pump wavelength of 1540 nm, for the fundamental quasi-TM mode shown in Fig. 5(a). From this, we estimate the dispersion length L_D=~27 cm to be considerably longer than the waveguide length L_{wg}=1.537 cm used in the nonlinear loss measurements. Therefore, the contribution of the dispersion on the pulse peak power is negligible. In this case, the intensity profile $I(z,t)$ of the pulse can be described by the two coupled equations given in Eqs. (2) and (3). For the known linear loss α_l of 4 dB cm^{-1}, we determined the TPA coefficient of the poly-Si waveguides by fitting to the nonlinear absorption data, solving the coupled equations. The remaining material parameters were estimated from the single crystal values of silicon in the literature, with the FCA coefficient of $\sigma_{FCA} = 1.45 \times 10^{-21}$ m^2 calculated via the Drude-Lorenz model. The resulting curve is plotted as the solid black line in Fig. 5(b). The simulations revealed that the best fit value for the TPA coefficient is $\beta_{TPA} = 9\times10^{-12}$ $m^2\,W^{-1}$, which is at the upper end of the range reported for c-Si ($\beta_{TPA} = 4.5\text{–}9\times10^{-12}$ $m^2\,W^{-1}$) [24-26]. We attribute this high TPA value to the residual tensile stresses, which can act to decrease the bandgap of the polycrystalline material, as well as the bandgap tails created by the amorphous content around the crystal grains. Finally, we should note that inter-pulse carrier accumulation effects were neglected for the simulations as the time interval between the pulses is sufficient for the material to recover (τ_c = ~1 ns < τ_p=*25* ns).

5.2. Spectral broadening by self-phase modulation

With the estimated values for the losses (β_{TPA} and α_l), characterization of the nonlinear properties of the poly-Si waveguides was completed by studying the SPM-induced spectral broadening of the pulses to determine the Kerr coefficient n_2. The original input spectrum and

output spectra of the pulses recorded by an optical spectrum analyzer (OSA) are shown in Fig. 6(a) and Fig. 6(b-d) for the input peak powers given in the legend. The value of n_2 was estimated by fitting the spectral broadening with numerical solutions to the full NLSE equation in Eq. (1), which is coupled to Eq. (2) describing the rate of change in the density of TPA-generated free carriers. Comparing the simulated spectral widths with the measured spectra, we found the best fit value of $n_2 = 4.5\times10^{-18}$ m W^{-1}, which is within the range of values measured for c-Si ($n_2 = 4.3–6\times10^{-12}$ m W^{-1}) [24-26]. It is worth noting that the only previous estimates of the nonlinear optical parameters of a poly-Si material were obtained using a poly-Si core fiber [22], where the nonlinear parameters were estimated to be $n_2 = 4.2\times10^{-12}$ m W^{-1} and $\beta_{TPA} = 7.5\times10^{-12}$ m^2 W^{-1} at a wavelength of 1540 nm. The simulated output spectra corresponding to the input peak powers are plotted as the black dashed curves in Fig. 6, showing a good qualitative agreement between the simulated and measured output spectra for all powers. As the pulse width is much shorter than the carrier lifetime, the effect of FCA on the symmetry of the spectral broadening is minimal [27], however, a small blue-shift is noticeable at the highest input peak power due to the effect of FCD, which was also observed in c-Si at telecom wavelengths [28]. We neglect contributions due to higher order dispersion because the 3 μm wide poly-Si waveguides exhibit relatively large normal GVD over the telecom wavelength region. Additionally, we didn't observe any high order multi-photon effects or thermal effects during the nonlinear measurements, as the maximum average power (50 mW) and wavelength (1540 nm) of the pulsed laser source render the contribution of these effects insignificant.

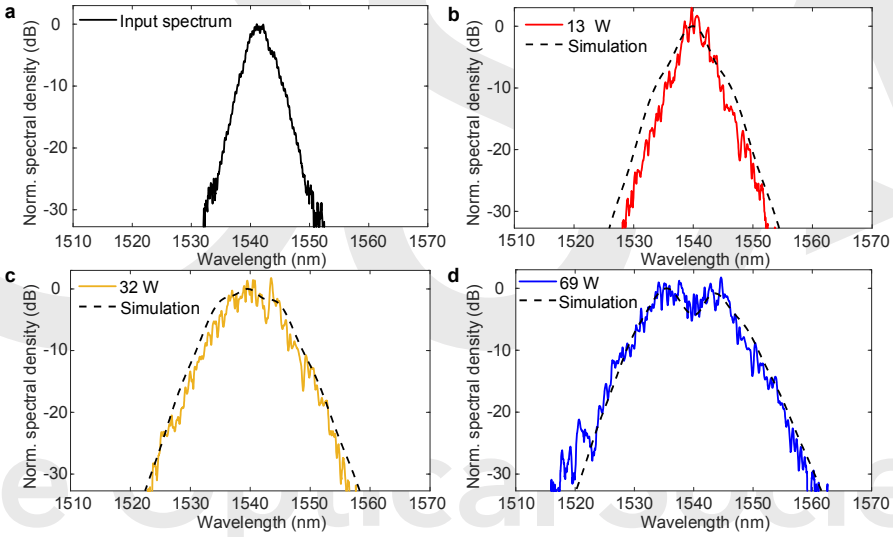

Fig. 6. Input-power-dependent spectral broadening in the laser-processed poly-Si waveguides due to SPM. (**a**) Original input spectrum. Output spectra taken for different input peak powers of (**b**) 13 W, (**c**) 32 W, and (**d**) 69 W. The simulated results obtained from the NLSE modelling with Eqs. (1,2) are represented by the fitted black dashed lines.

6. Conclusion

Our results have shown that laser post-processing of a-Si deposited on planar substrates is a promising approach to obtain poly-Si waveguides with optical losses low enough to observe third-order nonlinear effects, such as SPM, four-wave mixing (FWM) and cross-phase modulation (XPM). The nonlinear transmission measurements have revealed both the TPA parameter β_{TPA} and the nonlinear refractive index n_2 for the laser-processed poly-Si waveguides to be in the range expected for c-Si waveguides. This could be leveraged for various applications such as optical communications, signal processing, and spectroscopy in

integrated photonics circuits. Deposition of the a-Si at low temperatures complies with the low thermal budget required for CMOS processes and, by ensuring the heat required to crystallize the material stays local to the individual components, laser processing provides a route to fabricating high density nonlinear silicon circuits. Continuing efforts to enhance the material quality by laser processing will help to improve both the optical and electrical properties of poly-Si for the development of future integrated electronic/photonic chips.

Funding

Engineering and Physical Sciences Research Council (EPSRC) (EP/P000940/1 and EP/N013247/1).

Acknowledgments

The authors thank Dr. Joseph Campling and Dr. Yohann Franz for useful discussions. The data for this work is accessible through the University of Southampton Institutional Research Repository (https://doi.org/10.5258/SOTON/D1507).

Disclosures

The authors declare no conflicts of interest.

References

1. J. S. Orcutt, S. D. Tang, S. Kramer, K. Mehta, H. Li, V. Stojanović, and R. J. Ram, "Low-loss polysilicon waveguides fabricated in an emulated high-volume electronics process," Opt. Express **20**(7), 7243–7254 (2012).
2. D. Kwong, J. Covey, A. Hosseini, Y. Zhang, X. Xu, and R. T. Chen, "Ultralow-loss polycrystalline silicon waveguides and high uniformity 1x12 MMI fanout for 3D photonic integration," Opt. Express **20**(19), 21722–21728 (2012).
3. A. H. Atabaki, S. Moazeni, F. Pavanello, H. Gevorgyan, J. Notaros, L. Alloatti, M. T. Wade, C. Sun, S. A. Kruger, H. Meng, K. Al Qubaisi, I. Wang, B. Zhang, A. Khilo, C. V. Baiocco, M. A. Popović, V. M. Stojanović, and R. J. Ram, "Integrating photonics with silicon nanoelectronics for the next generation of systems on a chip," Nature **556**, 349–354 (2018).
4. Y. H. D. Lee, M. O. Thompson, and M. Lipson, "Deposited low temperature silicon GHz Modulator," Opt. Express **21**(22), 26688–26692 (2013).
5. K. Preston, B. Schmidt, and M. Lipson, "Polysilicon photonic resonators for large-scale 3D integration of optical networks," Opt. Express **15**(25), 17283–17290 (2007).
6. Q. Fang, J. F. Song, S. H. Tao, M. B. Yu, G. Q. Lo, and D. L. Kwong, "Low loss (~6.45dB/cm) sub-micron polycrystalline silicon waveguide integrated with efficient SiON waveguide coupler," Opt. Express **16**(9), 6425–6432 (2008).
7. F. Xia, L. Sekaric, and Y. Vlasov, "Ultracompact optical buffers on a silicon chip," Nat. Photonics **1**, 65–71 (2007).
8. K. Li, and A. C. Foster, "Nonlinear optics in hydrogenated amorphous silicon," IEEE J. Sel. Top. Quantum Electron. **24**(6), 8201212 (2018).
9. L. Wang, W. Xie, D. V. Thourhout, Y. Zhang, H. Yu, and S. Wang, "Nonlinear silicon nitride waveguides based on a PECVD deposition platform," Opt. Express **26**(8), 9645–9654 (2018).
10. J. S. Foresi, M. R. Black, A. M. Agarwal, and L. C. Kimerling, "Losses in polycrystalline silicon waveguides," Appl. Phys. Lett. **68**(15), 2052–254 (1996).
11. S. Zhu, G. Q. Lo, J. D. Ye, and D. L. Kwong, "Influence of RTA and LTA on the optical propagation loss in polycrystalline silicon wire waveguides," IEEE Photonics Technol. Lett. **22**(7), 480–482 (2010).
12. S. Zhu, Q. Fang, M. B. Yu, G. Q. Lo, and D. L. Kwong, "Propagation losses in undoped and n-doped polycrystalline silicon wire waveguides," Opt. Express **17**(23), 20891–20899 (2009).
13. L. Liao, D. R. Lim, A. M. Agarwal, X. Duan, K. K. Lee, and L. C. Kimerling, "Optical transmission losses in polycrystalline silicon strip waveguides: effects of waveguide dimensions, thermal treatment, hydrogen passivation, and wavelength," J. Electron. Mater. **29**(12), 1380–1386 (2000).
14. S. Cheemalapati, M. Ladanov, J. Winskas, and A. Pyayt, "Optimization of dry etching parameters for fabrication of polysilicon waveguides with smooth sidewall using a capacitively coupled plasma reactor," Appl. Opt. **53**(25), 5745–5749 (2014).
15. Y. Franz, A. F. J. Runge, S. Z. Oo, G. Jimenez-Martinez, N. Healy, A. Khokhar, A. Tarazona, H. M. H. Chong, S. Mailis, and A. C. Peacock, "Laser crystallized low-loss polycrystalline silicon waveguides," Opt. Express **27**(4), 4462–4470 (2019).
16. K. Kitahara, Y. Ohashi, Y. Katoh, A. Hara, and N. Sasaki, "Submicron-scale characterization of poly-Si thin films crystallized by excimer laser and continuous-wave laser," J. Appl. Phys. **95**(12), 7850–7855 (2004)

17. T. M. B. Masaud, A. Tarazona, E. Jaberansary, X. Chen, G. T. Reed, G. Z. Mashanovich, and H. M. H. Chong, "Hot-wire polysilicon waveguides with low deposition temperature," Opt. Lett. **38**(20), 4030–4032 (2013).
18. C.-H. Chou, I-C. Lee, P.-Y. Yang, M.-J. Hu, C.-L. Wang, C.-Y. Wu, Y.-S. Chien, K.-Y. Wang, and H.-C. Cheng, "Effects of crystallization mechanism on the electrical characteristics of green continuous-wave-laser-crystallized polycrystalline silicon thin film transistors," Appl. Phys. Lett. **103**, 053515 (2013).
19. F. Ureña, S. H. Olsen, and J.-P. Raskin, "Raman measurements of uniaxial strain in silicon nanostructures," J. Appl. Phys. **114**, 144507 (2013).
20. O. Aktas, S. Z. Oo, S. J. MacFarquhar, V. Mittal, H. M. H. Chong, and A. C. Peacock, "Laser-driven phase segregation and tailoring of compositionally graded microstructures in Si−Ge nanoscale thin films," ACS Appl. Mater. Interfaces **12**, 9457−9467 (2020).
21. J. F. Michaud, R. Rogel, T. Mohammed-Brahim, and M. Sarret, "CW argon laser crystallization of silicon films: structural properties," J. Non-Cryst. Solids **352**, 998–1002 (2006).
22. H. Ren, L. Shen, D. Wu, O. Aktas, T. Hawkins, J. Ballato, U. J. Gibson, and A. C. Peacock, "Nonlinear optical properties of polycrystalline silicon core fibers from telecom wavelengths into the mid-infrared spectral region," Opt. Mater. Express **9**(3), 1271–1279 (2019).
23. L. Yin and G. P. Agrawal, "Impact of two-photon absorption on self-phase modulation in silicon waveguides," Opt. Lett. **32**(14), 2031−2033 (2007).
24. R. Dekker, N. Usechak, M. Först, and A. Driessen, "Ultrafast nonlinear all-optical processes in silicon-on-insulator waveguides," J. Phys. D: Appl. Phys. **40,** R249–R271 (2007).
25. H. K. Tsang, and Y. Liu, "Nonlinear optical properties of silicon waveguides," Semicond. Sci. Technol. **23**, 064007 (2008).
26. K. Li, and A. C. Foster, "Parametric nonlinear silicon-based photonics," Proc. IEEE **106**(12), 2196–2208 (2018).
27. Q. Lin, O. J. Painter, and G. P. Agrawal, "Nonlinear optical phenomena in silicon waveguides: Modeling and applications," Opt. Express **15**(25), 16604–16644 (2007).
28. X. Liu, J. B. Driscoll, J. I. Dadap, and R. M. Osgood Jr., S. Assefa, Y. A. Vlasov, and W. M. J. Green, "Self-phase modulation and nonlinear loss in silicon nanophotonic wires near the mid-infrared two-photon absorption edge," Opt. Express **19**(8), 7778–7789 (2011).